Conformational Isomerization of the Fe(III)-OH Species Enables Selective Halogenation in Non-Heme Iron Halogenase BesD and Hydroxylase-Evolved Halogenase

Jinyan Zhang,[1,2] Yifan Li,[1] Wenli Yuan,[1] Xuan Zhang,[3] Yubing Si,[4] Binju Wang*[,1]

[1]State Key Laboratory of Physical Chemistry of Solid Surfaces and Fujian Provincial Key Laboratory of Theoretical and Computational Chemistry, College of Chemistry and Chemical Engineering and Innovation Laboratory for Sciences and Technologies of Energy Materials of Fujian Province (IKKEM), Xiamen University, Xiamen 361005, China

[2]Department of Chemistry, Institutes of Biomedical Sciences, and Shanghai Stomatological Hospital, Fudan University, Shanghai 200000, China

[3]Institute of Drug Discovery Technology, Ningbo University, Ningbo 315211, China

[4]College of Chemistry, Zhengzhou University, Zhengzhou 450001, China

KEYWORDS: non-heme iron halogenase, selective hydroxylation, QM/MM, conformational isomerization

ABSTRACT: Non-heme iron(II)/2-oxoglutarate (Fe/2OG)-dependent enzymes catalyze a large number of C-H bond activation and functionalization. Especially, non-heme iron halogenases catalyze the selective C-H halogenation, representing an attractive strategy for the biosynthesis of halogenated compounds. Despite extensive endeavors from experiments and computations, how non-heme iron halogenases dictate the reaction toward the thermodynamically unfavored halogenation is still elusive. Here, we have investigated the chlorination versus hydroxylation selectivity in both halogenase BesD and hydroxylase-evolved halogenase Chi-14, using extensive MD simulations and QM/MM calculations. In BesD, our calculations have shown that 2OG-assisted O_2 activation affords the axial Fe(IV)-oxo species that is responsible for the substrate C-H activation. To facilitate the following Cl-rebound reaction, the nascent axial Fe(III)-OH species has to undergo the conformational isomerization to the equatorial one. This can remove the steric effects between the axial Fe(III)-OH and the substrate radical, thereby facilitating the migration of substrate radical toward Cl-ligand during the Cl-rebound. Notably, the second-sphere residue Asn (Asn219 in BesD or Asn225 in Chi-14) can form persistent hydrogen bond interactions with succinate, which is vital to maintain the unsaturated five-coordination shell of Fe, thereby facilitating the conformational flip of Fe(III)-OH from the axial orientation to the equatorial one. Our findings agree with the available experimental information, highlighting the key role of the coordination dynamics of iron in dictating the catalysis of non-heme enzymes.

1.INTRODUCTION

Iron(II)-and 2-oxoglutarate-dependent (Fe/2OG) oxygenases catalyze a large variety of transformations that are essential for biosynthesis and metabolism functions.[1-8] Among various transformations, the selective C-H halogenation represents a valuable strategy for the biosynthesis of halogenated compounds.[9, 10] As the introduction of halogen can well modulate the chemical and biological properties of compounds, the halogenated compounds have found wide applications in medicines, pesticide, insecticide and so on. To date, a number of Fe/2OG halogenases have been identified, including SyrB2,[11, 12] CytC3,[13, 14] WelO5,[15-17] BesD[18-20] and AdaV.[21, 22]

The catalysis of Fe/2OG halogenases bear notable resemblances to those of Fe/2OG hydroxylases.[23-25] In both classes of enzymes, the reactions with substrates are typically initiated by hydrogen atom transfer (HAT) from the substrate C-H bond to the Fe(IV)-oxo active species, leading to the formation of the substrate radical.[26-31] Distinctively, the substrate radical in Fe/2OG hydroxylases proceeds with the OH-rebound to generate the hydroxylated product, while the substrate radical in Fe/2OG halogenases prefers to undergo Cl-rebound to form the halogenated product. However, how halogenases can dictate the halogenation selectivity but largely inhibit the thermodynamically favored hydroxylation activity is a long-standing debate.

Among various Fe/2OG halogenases, the catalytic mechanism of the carrier-protein-dependent SyrB2 has been most extensively studied to date. SyrB2 is responsible for the halogenation of L-threonine (L-Thr) that is covalently tethered as a thioester to the phosphopantetheine arm of its carrier protein, SyrB1.[11, 12, 32] Extensive studies have been conducted to unravel the molecular determinant in partitioning between halogenation vs. hydroxylation. Experimental investigations pinpointed that the substrate as a pivotal factor in ensuring halogenation specificity.[33] Meanwhile, computational studies have postulated several mechanisms

to elucidate the partitioning between halogenation vs. hydroxylation. These include: (a) Protonation of the Fe(III)-OH intermediate to inhibit the hydroxylation,[34] (b) Concomitant C-H activation and Cl-rebound, which diminishes the barrier of the halogenation reaction,[35] (c) The coordination isomerization of the Cl-Fe(IV)-oxo intermediate as shown in Scheme 1a-i, where the halogenation reaction is enhanced by the ligand swap between oxo and chloride. In such a mechanism, the equatorial Fe(IV)-oxo species performs HAT from the substrate C-H via a π-pathway;[36] (d) The coordination isomerization of the Cl-Fe(III)-OH intermediate as shown in Scheme 1a-ii, in which the axial Fe(IV)-oxo species perform HAT from the substrate C-H via a σ-pathway.[37] Then, the positional exchange between hydroxide and chloride ligands facilitates the halogenation reaction. Nonetheless, the absence of a definitive enzyme-substrate complex structure between SyrB2 and SyrB1 challenges the predictive capability of these computational models. For instance, the MD-predicted active site structure and hydrogen bonding networks of SyrB2 differ from those from the QM models guided by the spectroscopy information.[38-41]

Through comprehensive computational assessments and spectroscopic examinations,[38-40] Solomon and coworkers proposed a mechanism of SyrB2, depicted in in Scheme 1a-iii, in which the 2OG-assisted oxygen activation leads to the formation of the equatorial Fe(IV)-oxo species. The following HAT from the substrate C-H to the equatorial Fe(IV)-oxo species affords the equatorial Fe(III)-OH species. Intriguingly, the partitioning between halogenation vs. hydroxylation can be well rationalized by a mechanistic picture that both the Cl- and OH-rebound reactions involve the migration of the oxidized substrate towards either Cl^- or OH^- ligand.[38, 42] Compared to the OH^- ligand, the weaker ligand field of Cl^- results in a lower lying $\pi^*_{Fe\text{-}Cl}$ orbital for accepting electron. Consequently, electron transfer (ET) from the carbon radical to the Fe(III) center is kinetically favored in Cl-rebound than that of the OH-rebound. Nevertheless, recent MD simulations with the carry protein SyrB1 suggest that the axial Fe(IV)-oxo could be responsible for the C-H activation of the substrate in SyrB2.[41]

In addition to the carrier-protein-dependent SyrB2, several carrier-protein-independent halogenases have been structurally characterized, which afforded us a more robust platform to delve into the catalytic mechanism of Fe/2OG halogenases. Considering WelO5, a carrier-independent enzyme, QM/MM studies suggested that the nascent Fe(IV)-oxo species can form a strong hydrogen bond with the second-sphere residue Ser189, which brings the Fe(IV)-oxo species into an equatorial orientation during the process of O-O cleavage reaction (Scheme 1b).[42] Consequently, the substrate C-H activation ensues a π-pathway. In line with the findings of SyrB2, the Cl-rebound reaction is kinetically favored over that of the OH-rebound from the equatorial Fe(III)-OH intermediate. Besides, the carrier-independent BesD catalyzes the halogenation at the C4 site of lysine, the first step in the biosynthesis of the acetylenic amino acid, β-ethynylserine.[18, 20] The QM model calculations have advocated for the conformational isomerization of the axial Fe(IV)-oxo species to its equatorial counterpart, playing an instrumental role in both C-H bond activation and subsequent selective halogenation (Scheme 1c).[43] In a notable divergence, the recent MD simulations ruled out the involvement of the equatorial Fe(IV)-oxo species in BesD.[44]

Besides the native Fe/2OG halogenases, the engineered Fe/2OG halogenases from the corresponding Fe/2OG hydroxylases can achieve similar activity and selectivity as the related BesD, which not only expands the function of Fe/2OG hydroxylases, but also offers an invaluable opportunity to further dissect the structure-function relationship between the active site architecture and the halogenation selectivity.[45, 46]

In this work, combined MD simulations and QM/MM calculations have been conducted to probe the chlorination versus hydroxylation selectivity in both natural halogenase BesD and hydroxylase-evolved halogenase Chi-14. Our calculations show that 2OG-assisted O_2 activation leads to the formation the axial Fe(IV)-oxo species in BesD, which is responsible for the activation of the target C-H bond in both BesD and Chi-14. However, the axial conformation of Fe(III)-OH can largely prevent the rebound of the substrate radical to the Cl-ligand via the steric effects. Instead, the unsaturated five-coordination shell of Fe can facilitate the isomerization of Fe(III)-OH from the axial conformation to the equatorial one, thereby removing the steric effects and enhancing the desired chlorination reaction.

Scheme 1. Proposed Representative Mechanisms to Rationalize the Partitioning between Halogenation vs. Hydroxylation in Fe/2OG Halogenases[a]

(a) Previously proposed mechanism of SyrB2-catalyzed selective halogenation

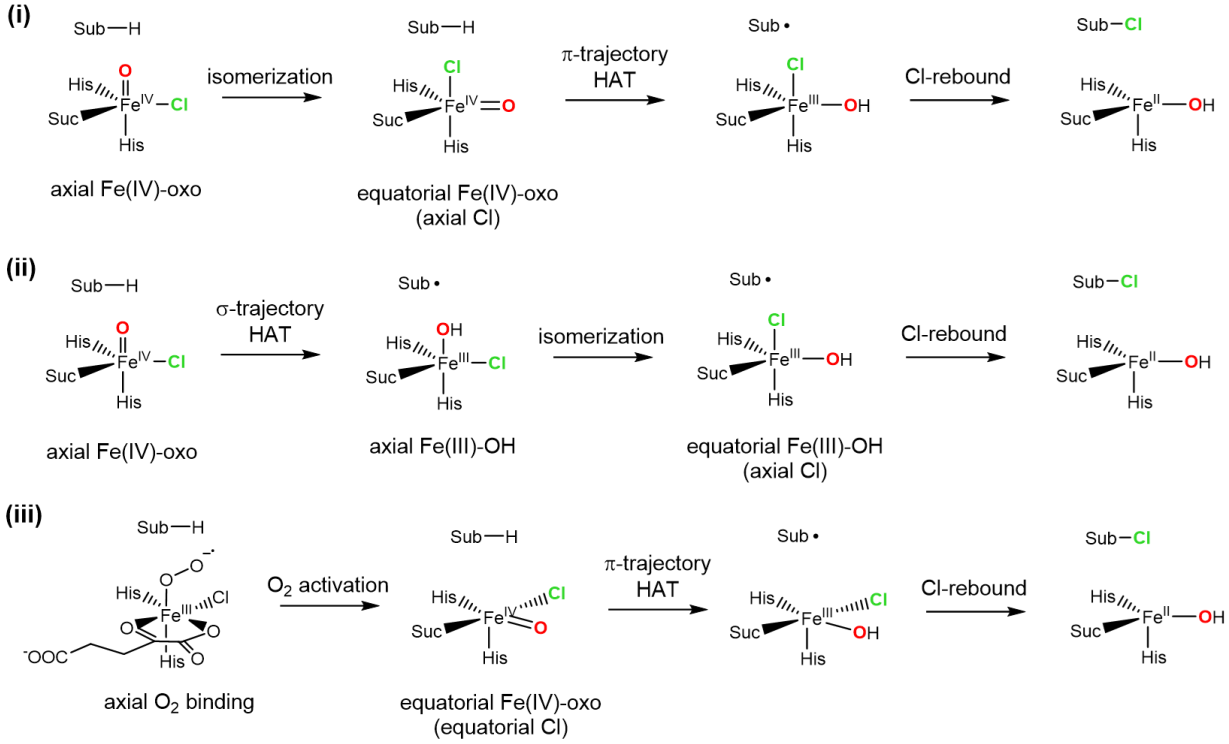

(b) Previously proposed mechanism of WelO5-catalyzed selective halogenation

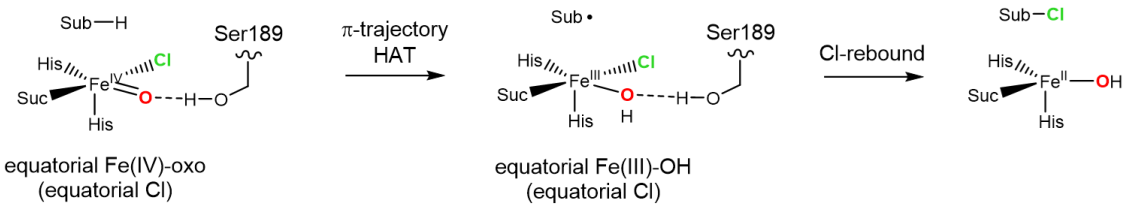

(c) Previously proposed mechanism of BesD-catalyzed selective halogenation

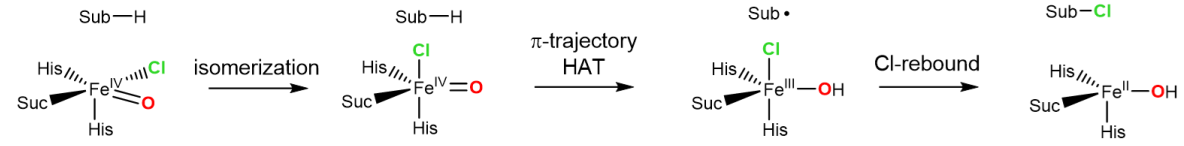

[a]The axial conformation is defined as the one in which the oxo/OH is pointing toward the substrate C-H, while the equatorial conformation is defined as the one in which the oxo/OH is pointing away from the substrate C-H.

2.METHODS

2.1 System Setup and MD simulations

For the wide-type BesD and the N219A mutant, the initial structure was prepared based on the crystal structure (PDB: 5C3Q). For O_2 activation, an oxygen molecule was added manually; for the following reaction, the active site was adjusted to Fe(IV)-oxo species. The protonation state of titratable residues was assigned on the basis of pKa values from PROPKA program[47] along with the local hydrogen-bonded networks of the residue. Histidine 28, 137, 165 and 204 were protonated at δ position, while histidine 42, 97, 113, 134 and 188 were protonated at ε position. All glutamic acid and aspartic acid residues were deprotonated.

The initial structure of Chi-14 with the axial Fe(IV)-oxo species was prepared based on the crystal structure of the

lysine hydroxylase (PDB: 7JSD),[46] in which the mutations of D144G, F150L, N151I, A219S, V220T, M223I, V225N, V226M, S227T, S229A, E231K, G235E and V237D were introduced. The protonation state of titratable residues was assigned on the basis of pKa values from PROPKA program[47] along with the local hydrogen-bonded networks. Histidine 64, 131, 142, 209 were protonated at δ position, while histidine 4, 41, 139, 170, 172 were protonated at ε position. All glutamic acid and aspartic acid residues were deprotonated.

For the MD simulations, the Amber ff14SB force field[48] was employed for the standard protein residues. The parameters of Fe(III)-O_2^- species and the Fe(IV)-oxo active site were obtained from the "MCPB.py" tool[49, 50] of AmberTools18.[51] The general AMBER force field (gaff)[52] was used to generate the parameters for the substrate, with the partial atomic charges obtained from the RESP calculations[53] at the B3LYP/6-31G(d) level of theory. The parmchk2 utility from AmberTools18 was used to generate the missing parameters of the substrate. All MD simulations were performed with the GPU version of Amber 18 package.[51] More details of MD simulations can be found in SI.

2.2 QM/MM calculations

Representative snapshots from MD simulations of wild-type BesD, N219A and Chi-14 were selected for QM/MM calculations. All QM/MM calculations were performed with ChemShell software,[54, 55] combining Turbomole[56] for the QM region and DL_POLY[57] for the MM region with the Amber force field. The electronic embedding scheme[58] was used to account for the polarizing effect of the enzyme environment on the QM region. Hydrogen link atoms with the charge-shift model were applied to treat the QM/MM boundary. The QM/MM system contains the whole protein and solvation waters within 8 Å of protein. During QM/MM geometry optimizations, the QM region was treated with the hybrid UB3LYP density functional,[59-61] which was demonstrated to be practical for non-heme enzymes.[62-74] For geometry optimization, the double-ζ basis set def2-SVP[75] (labeled as B1) was used. Transition states were located with relaxed potential energy surface scans followed by full TS optimizations using the dimer optimizer implemented in the DL-FIND code. The energies of all species were further corrected with a larger basis set def2-TZVP[75] (labeled as B2). For BesD, the QM region consists of residues and ligands that directly coordinate with iron center, N219, T221, water molecule and substrate; while for N219A of BesD, the QM region consists of residues and ligands that directly coordinate with the iron center and substrate. For Chi-14, the QM region consists of residues and ligands that directly coordinate with iron center, N225, E125, T227, water molecule and substrate. Dispersion corrections computed with Grimme's D3 method[76-78] were included in QM regions in all QM/MM calculations.

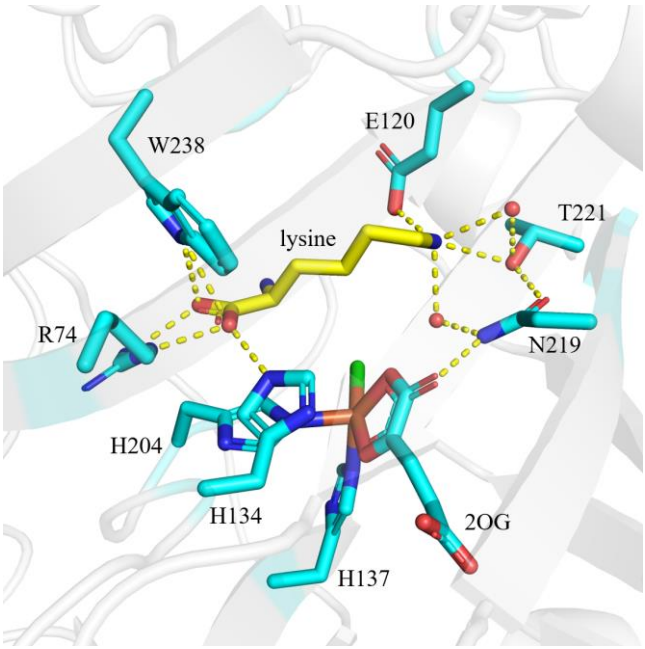

Figure 1. Active site of BesD (PDB: 5C3Q), where the substrate is highlighted with the yellow color.

3.RESULTS AND DISCUSSION

3.1 Active site structure of BesD

BesD is a carry-protein free Fe/2OG halogenase that chlorinates the amino acid lysine. BesD exhibits very low sequence similarity with the carry-dependent SyrB2 and the carry-independent WelO5. However, it shows high sequence similarity with certain hydroxylases.[19] The crystal structure of BesD in complex with the substrate lysine has been successfully characterized (Figure 1),[19] where Fe is ligated to His137, His204, chloride and 2OG. Meanwhile, the substrate lysine forms extensive hydrogen bonding networks with surrounding residues. Especially, the carboxyl group of the substrate is anchored by hydrogen bonding interactions with Arg74, His134 and Trp238, while the terminal amine is Hydrogen bonded to Glu120, Asn219 and Thr221. Moreover, the highly conserved Asn219 forms hydrogen bond interactions with 2OG. Experimental findings revealed that the N219A mutation obliterated halogenation selectivity, underscoring the pivotal role of N219 in steering the halogenation pathway.

3.2 Catalytic mechanism of BesD

3.2.1 Generation of the Fe(IV)-oxo active species

The mechanism of oxygen activation and formation of Fe(IV)-oxo species have been extensively studied before. It is recognized that the conformation of the nascent Fe(IV)-oxo species is key to the reaction partitioning between halogenation and hydroxylation. Previous computational studies suggested that the 2OG-assisted O_2 activation led to the equatorial Fe(IV)-oxo in SyrB2.[38, 40] Moreover, nuclear resonance vibrational spectroscopy (NRVS) and DFT calculations also suggested that the equatorial configuration of Fe(IV)-oxo was responsible for HAT in SyrB2.[38-40] Furthermore, QM/MM calculations have posited that the 2OG-assisted O_2 activation in WelO5 led to the equatorial Fe(IV)-oxo species in the quintet state.[42]

Due to the above considerations, we revisited the 2OG-assisted O_2 activation in BesD with QM/MM calculations. As depicted in Figure 2, our calculations are focused on the quintet state, which has been identified as the most reactive state for O_2 activation across previous studies.[79-86] In line with previous computational studies, the reaction is initiated by the attack of Fe(III)-superoxo species onto the 2OG, which is coupled to the C-C cleavage, affording a fresh CO_2 molecule and a Fe(II)-peracid intermediate in IC1. Next, the side-product of CO_2 was removed from the system and the Fe(II)-catalyzed reductive cleavage of O-O bond was investigated. It is seen that the O-O cleavage leads to the axial configuration of Fe(IV)-oxo species in IC2. As further illustrated in Figure 2, N219 maintains an hydrogen bond with succinate throughout the reaction pathway. Significantly, there are no discernible hydrogen bonding interactions between Fe(IV)-oxo and N219 in IC2. Hence, our QM/MM calculations clearly confirm the emergence of an axial Fe(IV)-oxo species in BesD following 2OG-assisted O_2 activation.

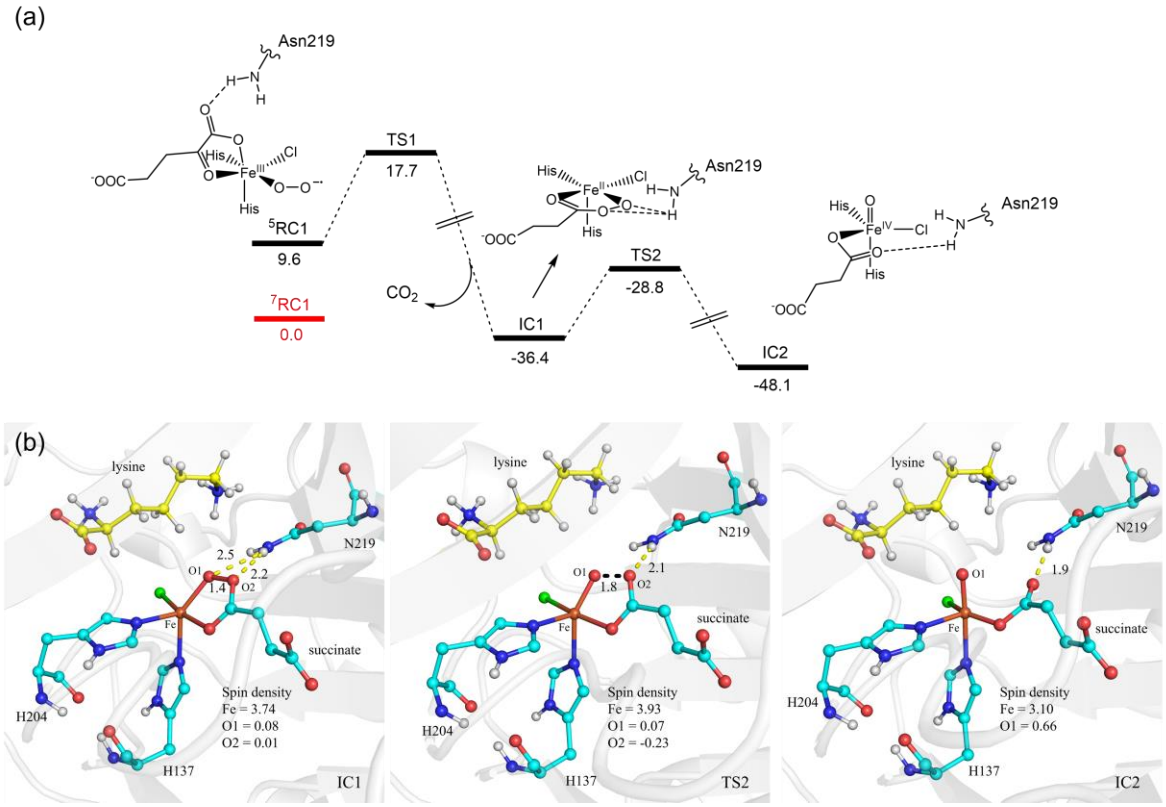

Figure 2. (a) QM(UB3LYP-D3/B2)/MM calculated energy profile (in kcal mol^{-1}) for the 2OG-assisted O_2 activation in BesD in the quintet state. (b) QM(UB3LYP-D3/B1)/MM optimized structures of key species involved in the reaction. Key distances are given in Å.

3.2.2 Coordination isomerization of the Fe(IV)-oxo intermediate

Coordination isomerization of the Fe(IV)-oxo intermediate has been widely proposed in previous computational studies.[87-89] Specifically, in BesD, recent QM model calculations postulated that the coordination isomerization of the Fe(IV)-oxo intermediate can bring the substrate C4-H closer to the Fe(IV)-oxo species (see Scheme 1c), thereby facilitating the following C-H activation.[43] However, the omission of the protein environment in QM model calculations may lead to the biased structures and energetics for enzymatic reactions. For instance, QM model calculations led to the spontaneous proton transfer from the substrate -NH_3^+ group to Glu120 in all optimized structures.[43] Additionally, the substrate positioning from the QM model calculations varies significantly with the crystal structure and the one from our QM/MM calculations (Figure S1).

Originating from the axial Fe(IV)-oxo species, our QM/MM calculations delineate that the isomerization of the Fe(IV)-oxo species from the axial configuration to the equatorial one requires a barrier of 9.2 kcal mol^{-1}, suggesting the process is quite kinetically favorable. In addition, the so-formed equatorial Fe(IV)-oxo species is only 1.7 kcal mol^{-1} higher than the axial one, suggesting both configurations of Fe(IV)-oxo species may exist in equilibrium. In the equatorial Fe(IV)-oxo species ($RC2_{eq}$ in Figure 3), it is apparent that the C4-H is 4.6 Å away from the Fe(IV)-oxo species, demonstrating that the direct C4-H bond activation by the equatorial Fe(IV)-oxo species could be unfavorable kinetically. Indeed, we have explored the HAT from the C4 site to the equatorial Fe(IV)-oxo configuration. However, the equatorial Fe(IV)-oxo evolved into the axial one during the QM/MM scanning (Figure S2), indicating that the equatorial Fe(IV)-oxo species is a dead-end and not reactive for C-H bond activation.

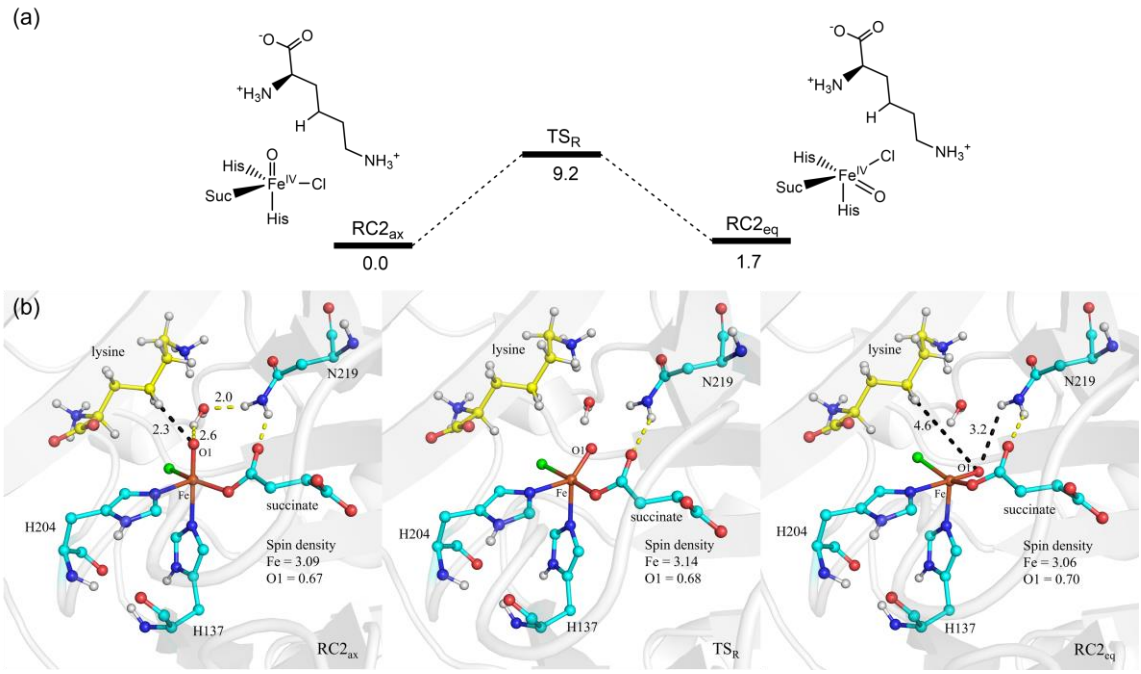

Figure 3. (a) QM/MM calculated energy profile (in kcal mol^{-1}) for the configurational isomerization of axial Fe(IV)-oxo to the equatorial Fe(IV)-oxo. (b) QM(UB3LYP-D3/B1)/MM optimized structures of key species involved in the reaction. Key distances are given in Å.

3.2.3 Reactivity of the axial vs. equatorial Fe(IV)-oxo species from MD analysis.

To further gauge the reactivity of the axial vs. equatorial Fe(IV)-oxo species in HAT from the C4 site of the substrate, we have compared the positioning of substrate C-H bonds relative to the axial Fe(IV)-oxo and the equatorial Fe(IV)-oxo species from MD simulations (Figure 4). For the axial Fe(IV)-oxo species, the MD-predicted average distance between the oxo and the target C4-H distance is ~3.3 Å, which is a suitable proximity for the subsequent HAT process. Moreover, within this configuration, the C4-H bond stands out by being the nearest to the Fe(IV)-oxo moiety compared to the other C-H bonds of the substrate (see Figure 4A). This finding points towards that the C4-H bond can be selectively activated. On the contrary, in the context of equatorial Fe(IV)-oxo species, the MD-predicted average distance between the oxo and the target C4-H distance is ~4.8 Å, suggesting the equatorial Fe(IV)-oxo is much less reactive in C-H bond activation than its axial counterpart. Collectively, these computational insights suggest that the axial Fe(IV)-oxo is responsible for the C-H activation of the substrate. A notable observation from our MD simulations is that Asn219 does not form the hydrogen bonding interaction with either axial or equatorial Fe(IV)-oxo group, but maintains the persistent hydrogen bonding interaction with the carboxyl group of succinate (Figure S3).

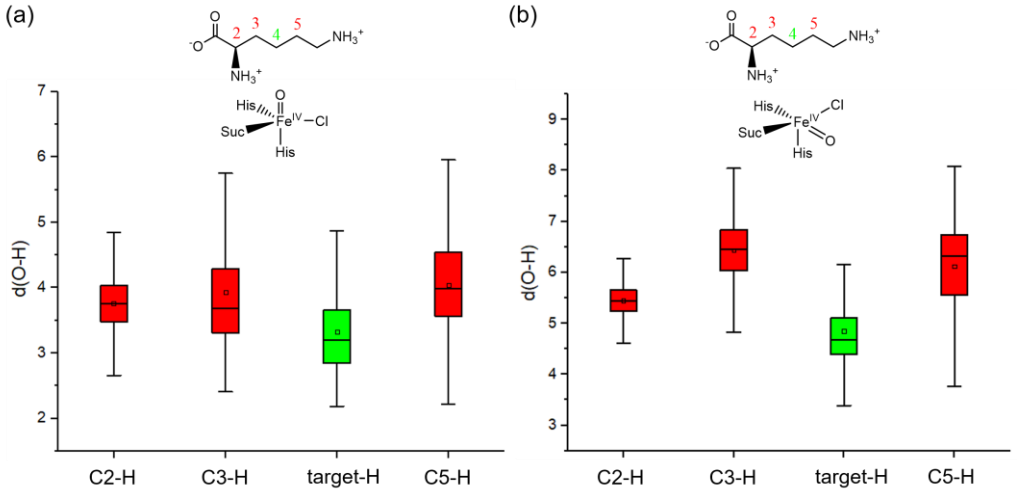

Figure 4. Distance fluctuation (in Å) between the different C-H bonds of the substrate and (a) the axial Fe(IV)-oxo species vs. (b) the equatorial Fe(IV)-oxo species during 100 ns MD simulations. The top and bottom boundaries of the box represent the

third (Q3) and first quartiles (Q1), respectively. The central horizontal lines inside the box denote the median, representing the middle value of the dataset. Small squares within the box marks represent the mean value of the data.

3.2.4 Chlorination vs. hydroxylation from the axial Fe(IV)-oxo species in BesD

In this section, we proceed to investigate the chlorination vs. hydroxylation reactivity from the axial Fe(IV)-oxo species. The axial configuration ($RC2_{ax}$ in Figure 3b), with its ideal proximity of the C4-H bond to the Fe(IV)-oxo species (2.3 Å), is ideal for the C-H bond activation. Population analysis shows that the HAT follows a σ-pathway, suggesting the HAT can be enhanced by the spin-exchange interactions within d-block of Fe.[80, 90-93] As shown in Figure 5, the HAT from C4-H to Fe(IV)-oxo species requires a barrier of 19.7 kcal mol^{-1}, leading to a Fe(III)-OH species (IC3) that is directed toward the C4 radical center. Starting from IC3, three potential pathways were explored. One is the Cl-rebound to the C4-radical via $TS4_{Cl}$ (illustrated in blue), en route to the chlorinated product. It is seen that the direct Cl-rebound pathway requires a high barrier of 33.5 kcal mol^{-1} relative to $RC2_{ax}$ and can be ruled out. The second pathway in black corresponds to the OH-rebound to the C4 radical, forming the hydroxylated product. This pathway has a barrier of 17.4 kcal mol^{-1} relative to $RC2_{ax}$ (illustrated in red), which is much favored over the Cl-rebound pathway kinetically. In the third pathway (illustrated in black), we found the Fe(III)-OH species can undergo a conformational change via TS4, which brings the OH ligand from its axial position to the equatorial position (IC4). Such isomerization demands a barrier of 13.3 kcal mol^{-1}, which is kinetically more favorable than the other two pathways (direct Cl-rebound via $TS4_{Cl}$ and OH-rebound via $TS4_{OH}$).

Starting from IC4, we found the following Cl-rebound reaction is facile, with a barrier of 15.0 kcal mol^{-1} relative to $RC2_{ax}$ Obviously, the conformational change of Fe(III)-OH followed by the Cl-rebound is the most favorable pathway (the black profile). According to the QM/MM energy profiles in Figure 5, the Cl-rebound pathway via TS5 is 2.4 kcal mol^{-1} lower than that of the OH-rebound pathway via $TS4_{OH}$. This energy difference corresponds to an chlorination selectivity of approximately 98%, aligning reasonably well with the experimental observation of ~77%.[19] To further validate the mechanistic picture demonstrate in Figure 5, an alternative snapshot from MD simulation was examined with the QM/MM study (Figure S4), wherein the hydrogen bonding network of lysine NH_3^+ group varies with the one in Figure 5. Notably, this variant configuration consistently reflected the energy and selectivity trends observed in Figure 5. To further confirm this conclusion, we have tested other popular DFT functions for Fe-containing systems, including TPSSh,[94, 95] M06,[96] PBE0,[97] BP86.[98, 99] All these DFT functionals resonated with our primary conclusion, emphasizing the kinetic preference of chlorination over hydroxylation (Table S1).

A left question is why the conformational change of the Fe(III)-OH species can enhance the Cl-rebound reaction so remarkably. Inspection of the structural evolution from IC4 to TS5 within the favored Cl-rebound pathway provides valuable insight. A notable observation is the modest alteration in the Fe-Cl bond length during the Cl-rebound transition (transitioning from 2.4 Å in IC4 to 2.5 Å in TS5). Conversely, there is a more pronounced shift in the C4-Cl distance, which contracts from 3.8 Å in IC4 to 2.4 Å in TS5. This shift indicates that the Cl-rebound mechanism is predominantly governed by the migration of the substrate radical towards the chloride. In the context of the structure represented by IC3, the axial OH ligand is oriented directly towards the C4-radical. This geometric arrangement could potentially impose steric constraints, restricting the mobility of the substrate radical. Under these spatial limitations, the movement of the radical towards the chloride for the Cl-rebound becomes sterically hindered, rendering the process kinetically less favorable. This realization emphasizes the pivotal role of conformational isomerization of ligands in dictating reaction pathways and their associated energy barriers.

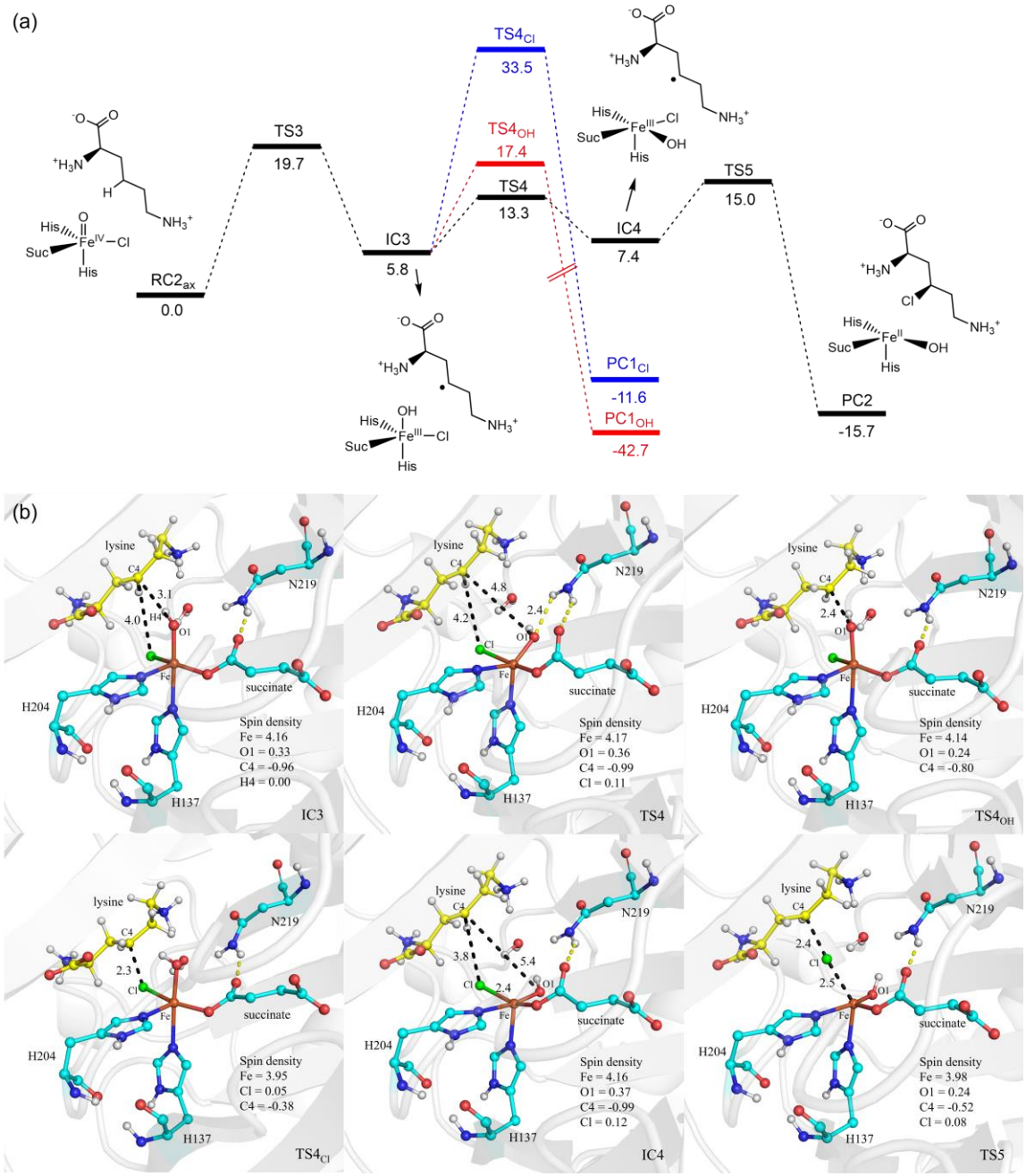

Figure 5. (a) QM(UB3LYP-D3/B2)/MM calculated energy profile (in kcal mol^{-1}) for the axial Fe(IV)-oxo mediated hydroxylation vs. chlorination in BesD in the quintet state. (b) QM(UB3LYP-D3/B1)/MM optimized structures of key species involved in the reaction. Key distances are given in Å.

3.2.5 Main roles of N219 in dictating the chlorination in BesD

Experiments have demonstrated that the N219A mutation leads to a loss of chlorination reactivity, underscoring the significance of the N219 residue in mediating selective chlorination.[19] To unravel the pivotal role of N219, we carried out QM/MM calculations on the N219A mutant (Figure 6). In contrast to wide-type enzyme, QM/MM MD simulations have revealed that the succinate maintains a bidentate coordination mode with Fe, leading to a six-coordinated Fe in the Fe(IV)-oxo species (Figure S5). Indeed, QM/MM scanning of breaking one Fe-O bond shows that the energy can increase steadily (Figure S6).

Beginning with RC3, the HAT from the substrate to the axial Fe(IV)-oxo requires a barrier of 20.9 kcal mol^{-1} and forms the Fe(III)-OH and substrate radical in IC5. This computed barrier of 20.9 kcal mol^{-1} is comparable to the value of 19.7 kcal mol^{-1} obtained from the five-coordinated Fe(IV)-oxo (Figure 5), suggesting that the coordination mode of succinate may have minor effects on the reactivity of Fe(IV)-oxo species. Proceeding from IC5, three possible routes have been compared (Figure 5). Unlike the wild-type enzyme, it is seen that the most favorable pathway corresponds to the OH-rebound, which involves a barrier of 10.8 kcal mol^{-1} relative to RC3 and leads to the formation of hydroxylated product. Interestingly, the isomerization of

the Fe(III)-OH species, transitioning from an axial to an equatorial orientation, is considerably less favorable in this context, with a barrier of 27.2 kcal mol^{-1} relative to RC3. In the N219A mutant, distinct from the wild-type enzyme, the hydrogen bonding interaction between N219 and succinate is eliminated, leaving no space to accommodate the flipped OH group. Thus, this second-sphere residue, vital for sustaining the unsaturated five-coordination state of the Fe(IV)-oxo, plays a crucial role in the conformational isomerization of the Fe(III)-OH species. Notably, the role of this hydrogen bond from Asn219 in BesD differs from that of the Ser189 proposed in WelO5. In the latter case,[16, 42] the hydrogen bond is mainly involved to stabilize the equatorial configuration of Fe(IV)-oxo species, instead of maintaining the single coordination mode of succinate.

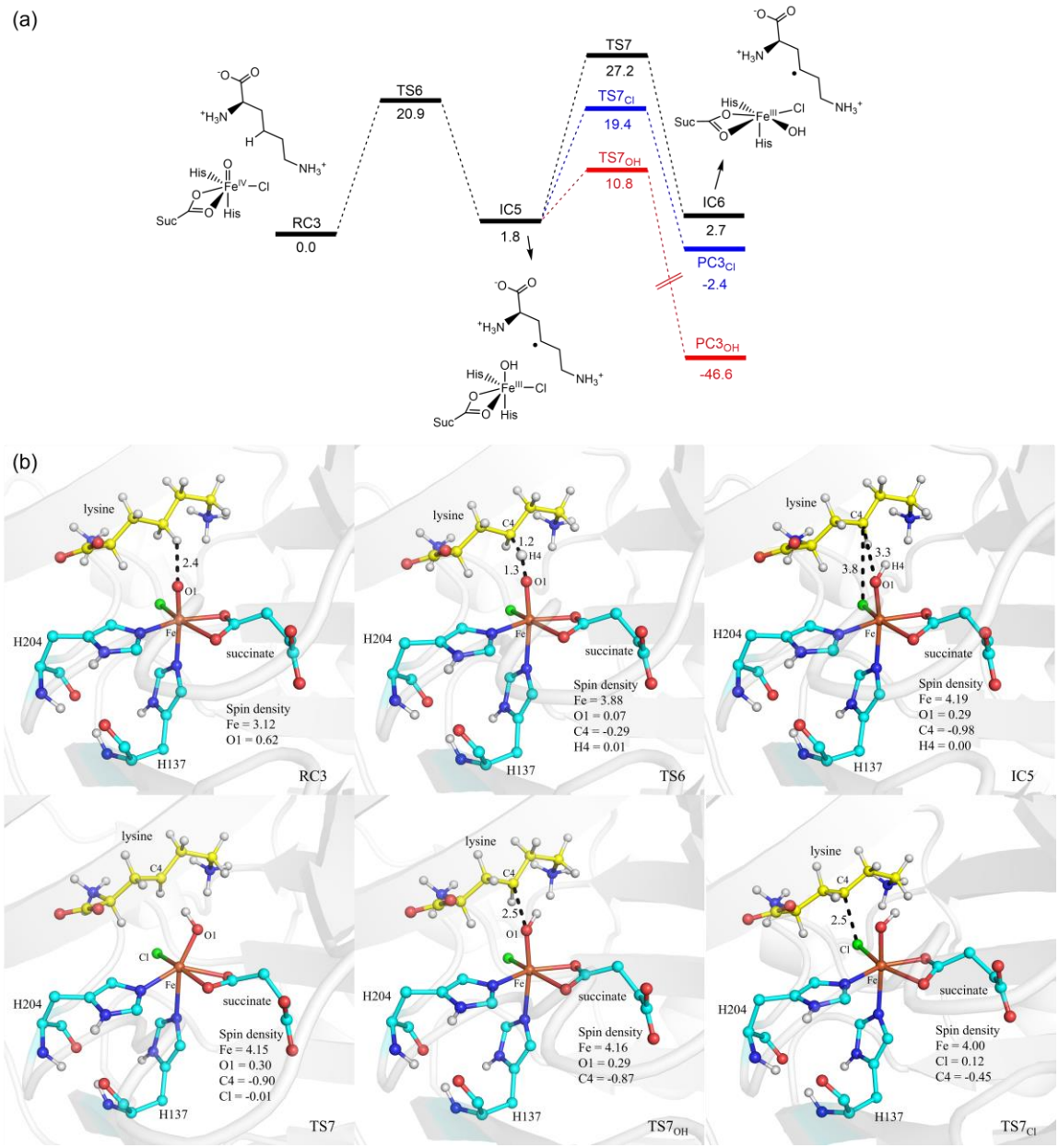

Figure 6. (a) QM(UB3LYP-D3/B2)/MM calculated energy profile (in kcal mol^{-1}) for the axial Fe(IV)-oxo mediated hydroxylation vs. chlorination in BesD-N219A in the quintet state. (b) QM(UB3LYP-D3/B1)/MM optimized structures of key species involved in the reaction. Key distances are given in Å.

3.3 chlorination vs. hydroxylation from the axial Fe(IV)-oxo species in Chi-14

In a recent experiment, a lysine hydroxylase has been characterized, which shares high sequence similarity with a halogenase from *Actinoplanes teichomyceticus*, who owns 51% similarity with BesD.[46] Using this lysine hydroxylase as template, 13 highly conserved residues of BesD were grafted into the D144G mutant of lysine hydroxylase, resulting in the variant named Chi-14 that is highly reactive and selective for lysine chlorination. Among 14 mutants, N225 that positioned in proximity to the Fe(IV)-oxo/Fe(III)-OH was demonstrated to be vital to the selective

chlorination reaction. Such the role of N225 could be analogous to that of N219 in BesD.

To further support the mechanistic scenario demonstrated in BesD, we further conducted the MD simulation and QM/MM calculations on Chi-14 catalyzed lysine chlorination (Figure 7 & Figure S7). Inspection of Figure 7A shows the mechanism of Chi-14 catalyzed lysine chlorination is quite similar to that of the BesD-catalyzed one. Here, the HAT from the substrate C4-H to Fe(IV)-oxo species forms the substrate radical and axial Fe(III)-OH species (IC7). Starting from IC7, the optimal pathway involves the flip of the OH-ligand to the equatorial position, which removes the steric effects to facilitate the Cl-rebound reaction, leading to the selective chlorination. Especially, N225 forms a hydrogen bond with succinate (Figure 7B), which is essential to maintain the five-coordinate architecture of Fe. Similar to the case of BesD, the five-coordinate architecture of Fe can facilitate the isomerization of the Fe(III)-OH species from the axial conformation to the equatorial one, leading to the selective chlorination. According to the QM/MM energy profiles in Figure 7, the Cl-rebound pathway via TS10 is 2.8 kcal mol^{-1} lower than that of the OH-rebound pathway via $TS9_{OH}$, which corresponds to a selectivity of ~99% in favor of chlorination. Such prediction is in qualitative agreement with a value of ~90%.[46] All these findings further validate the mechanistic scenario demonstrated in BesD.

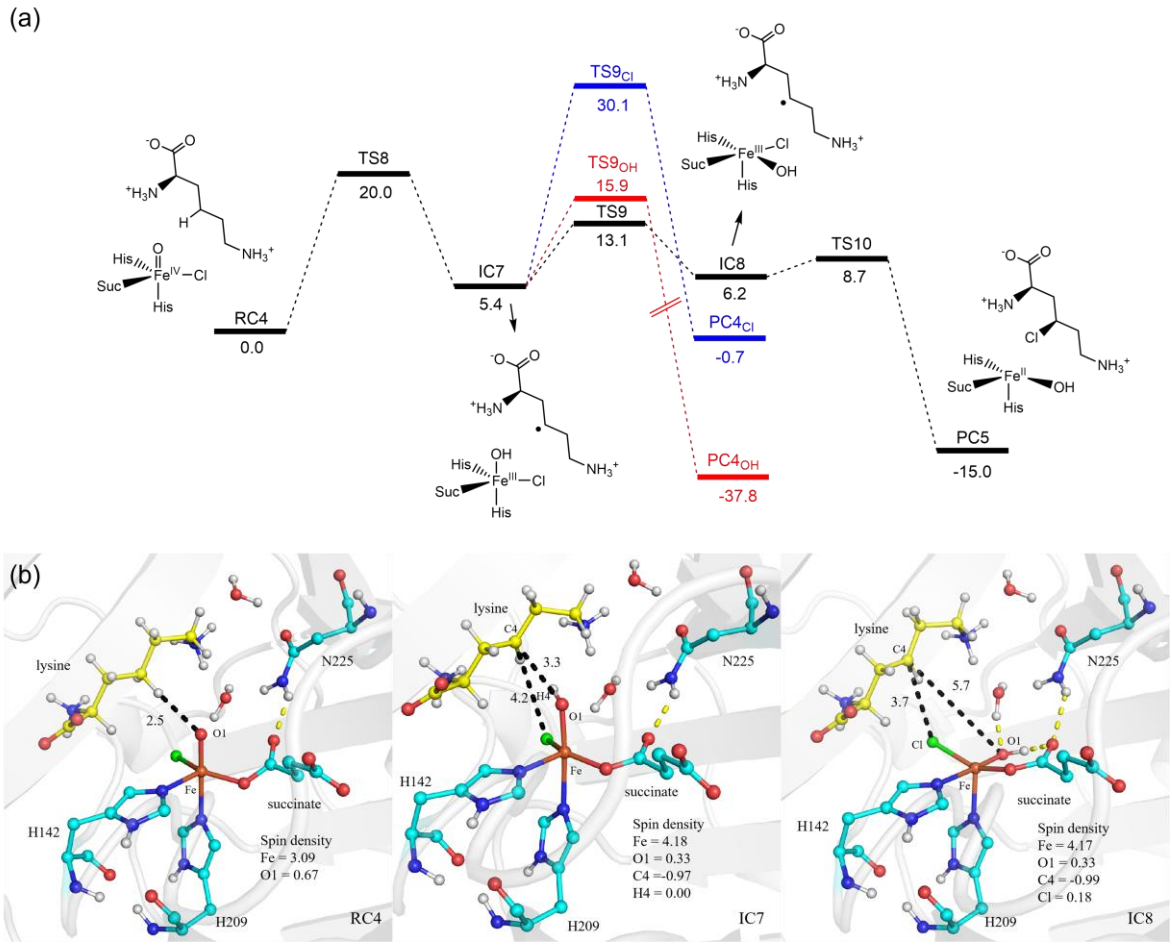

Figure 7. (a) QM(UB3LYP-D3/B2)/MM calculated energy profile (in kcal mol^{-1}) for the axial Fe(IV)-oxo mediated hydroxylation vs. chlorination in Chi-14 in the quintet state. (b) QM(UB3LYP-D3/B1)/MM optimized structures of key species involved in the reaction. Key distances are given in Å.

3.4 Proposed Catalytic Cycle of BesD and Chi-14

Drawing from the extensive simulations we have conducted, we proposed a catalytic cycle of BesD and Chi-14 in selective chlorination (Scheme 2). Our calculations show that 2OG-assisted O_2 activation affords the axial Fe(IV)-oxo species (**3**) in BesD, which is well directed toward the target C-H bond in both BesD and Chi-14. The further HAT from the substrate C-H to the axial Fe(IV)-oxo species culminates in the generation of the substrate radical and the axial Fe(III)-OH species (**4**) that is directed toward the carbon radical center of the substrate. From such axial conformation of Fe(III)-OH, the steric effects between the axial Fe(III)-OH and the substrate would prevent the substrate radical from approaching the Cl-ligand, thereby leading to the significantly high barrier for the Cl-rebound reaction. Instead, the unsaturated five-coordination shell of Fe can facilitate the isomerization of the Fe(III)-OH from the axial conformation to the equatorial one (**4**→**5**). The subsequent Cl-rebound (**5**→**6**) was demonstrated to be

quite facile in the equatorial Fe(IV)-oxo, as the steric effects involving the migration of the substrate radical to Cl-ligand can be depleted. Our study has shown that the second-sphere residue Asn (Asn219 in BesD or Asn225 in Chi) plays vital roles in maintaining the five-coordination shell of Fe, which in turn, permits the isomerization of Fe(III)-OH, transitioning it from an axial to an equatorial orientation. Especially, our QM/MM-predicted partitioning between chlorination vs. hydroxylation are in good agreement with the experiments in both BesD and Chi-14. Interestingly, the generation of the equatorial Fe(III)-OH intermediate correlates with the detailed computational analysis in SyrB2.[39, 40] In WelO5, the nascent Fe(IV)-oxo species can form a strong hydrogen bond with the second-sphere residue Ser189, which brings the Fe(IV)-oxo species to the equatorial position spontaneously. The further HAT from the substrate C-H to the equatorial Fe(IV)-oxo species can afford the equatorial Fe(III)-OH species directly in WelO5.[42]

While these aforementioned Fe/2OG halogenases all appear to converge on the shared equatorial Fe(III)-OH intermediates, it is elusive which configuration of species (axial vs. equatorial) is responsible for the C-H bond in SyrB2, as the exact substrate positioning has not been determined in SyrB2. For instance, the substrate positioning and the active site hydrogen bonding networks vary in different computational models.[36-38, 41] Drawing from insights in our current study, as well as prior research,[42] the configuration of Fe(IV)-oxo for the substrate C-H bond activation could be dependent on the substrate positioning. A flexible substrate binding may enable the approximation of substrate C-H to the equatorial Fe(IV)-oxo species, as suggested in WelO5. Otherwise, if the substrate is rigidly constrained by the hydrogen bonding network, it would be less unlikely for the equatorial Fe(IV)-oxo to be responsible for the C-H activation, as demonstrated in BesD and Chi-14.

To date, nearly all identified natural halogenases contain a second sphere residue that is found to be crucial for the selective halogenation, such as Arg247 in CurA,[100] Ser189 in WelO5,[16, 42] and Asn219 in BesD.[19] For these non-heme halogenases, mutations affecting these residues invariably diminish halogenation selectivity, hinting at a shared functional significance across these enzymes, as illustrated in BesD. In contrast to Fe/2OG halogenases, it appears that the unsaturated five-coordination geometry is inessential for C-H hydroxylation by Fe/2OG hydroxylases. Nevertheless, there are evidences to support a five-coordination geometry of Fe(IV)-oxo in Fe/2OG hydroxylases, such as taurine dioxygenase (TauD).[31] Meanwhile, a six-coordination geometry of Fe(IV)-oxo with an additional water ligand has been proposed in the non-heme AsqJ.[88] According to the computations, a water coordination to Fe can lead to a better agreement with the experimental spectroscopy.[13, 14, 26, 28, 101, 102] However, diverging from Fe/2OG halogenases, the role of the coordination geometry in Fe/2OG hydroxylases remains elusive and necessitates further investigation.

Scheme 2. Proposed Catalytic Cycle of BesD and Chi-14 in Selective Chlorination

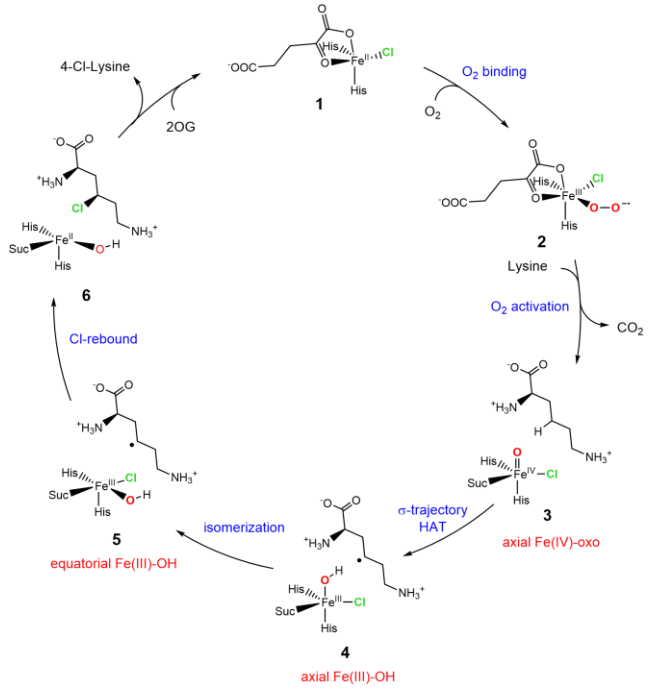

4.CONCLUSIONS

In summary, the combined MD simulations and QM/MM calculations have been performed to investigate the halogenation mechanism in both non-heme iron halogenase BesD and hydroxylase-evolved halogenase Chi-14. In both enzymes, the reliable substrate positioning can be obtained from the crystal structure and MD simulations. Both QM/MM calculations and MD simulations support that the axial Fe(IV)-oxo species is responsible for the substrate C-H activations, while the equatorial Fe(IV)-oxo species is a dead-end and not reactive for C-H bond activation. The further HAT from the substrate C-H to the axial Fe(IV)-oxo species forms the substrate radical and the axial Fe(III)-OH species. However, the steric effects between the axial Fe(III)-OH and the substrate would prevent the substrate radical from approaching the Cl-ligand, thereby leading to the significantly high barrier for the Cl-rebound reaction. To facilitate the following Cl-rebound reaction, the nascent axial Fe(III)-OH species has to undergo the conformational isomerization to the equatorial one, which will remove the steric effects between the axial Fe(III)-OH and the substrate radical, thereby facilitating the migration of substrate radical toward $Cl^{\cdot}$ ligand during the Cl-rebound. Especially, the second-sphere residue Asn (Asn219 in BesD or Asn225 in Chi-14) was demonstrated to be vital in maintaining the five-coordination shell of Fe, which facilitates the conformational flip of Fe(III)-OH from the axial direction to the equatorial one. This mechanistic interpretation is further supported by the QM/MM study of the N219A mutant of BesD, in which the removal of the hydrogen bonding interaction between N219 and succinate leads to the bidentate coordinate of succinate, inhibiting the conformational flip of Fe(III)-OH. These findings also have implications on the other non-heme Fe/2OG catalyzed C-H functionalization beyond the hydroxylation, such as the C-N bond formation,[103-105] C-S bond formation,[106, 107] C-C bond formation,[108-112] as well as the C-O bond formation,[113-121] in which the thermodynamically favored hydroxylation reactions have been inhibited.

ASSOCIATED CONTENT

Supporting Information
Tables S1, Figures S1–S6, computational details, and cartesian coordinates of QM region from QM/MM calculations (PDF). This material is available free of charge via the Internet at http://pubs.acs.org.

Corresponding Author

Binju Wang – *State Key Laboratory of Physical Chemistry of Solid Surfaces and Fujian Provincial Key Laboratory of Theoretical and Computational Chemistry, College of Chemistry and Chemical Engineering and Innovation Laboratory for Sciences and Technologies of Energy Materials of Fujian Province (IKKEM), Xiamen University, Xiamen 361005, P. R. China*; orcid.org/0000-0002-3353-9411

*E-mail: wangbinju2018@xmu.edu.cn

Author Contributions

All authors have given approval to the final version of the manuscript.

Notes

Any additional relevant notes should be placed here.

ACKNOWLEDGMENT

This work was supported by the National Natural Science Foundation of China (No. 22122305, 22073077 and 21933009)

REFERENCES

(1) Farrow, S. C.; Facchini, P. J. Functional diversity of 2-oxoglutarate/Fe(II)-dependent dioxygenases in plant metabolism. *Front. Plant Sci.* **2014**, *5*.
(2) Martinez, S.; Hausinger, R. P. Catalytic Mechanisms of Fe(II)- and 2-Oxoglutarate-dependent Oxygenases. *J. Biol. Chem.* **2015**, *290* (34), 20702-20711.
(3) Wu, L. F.; Meng, S.; Tang, G. L. Ferrous iron and α-ketoglutarate-dependent dioxygenases in the biosynthesis of microbial natural products. *Biochim. Biophys. Acta. Proteins Proteom.* **2016**, *1864* (5), 453-470.
(4) Herr, C. Q.; Hausinger, R. P. Amazing Diversity in Biochemical Roles of Fe(II)/2-Oxoglutarate Oxygenases. *Trends Biochem. Sci* **2018**, *43* (7), 517-532.
(5) Ushimaru, R.; Abe, I. Unusual Dioxygen-Dependent Reactions Catalyzed by Nonheme Iron Enzymes in Natural Product Biosynthesis. *ACS Catal.* **2022**, 1045-1076.
(6) Solomon, E. I.; Brunold, T. C.; Davis, M. I.; Kemsley, J. N.; Lee, S.-K.; Lehnert, N.; Neese, F.; Skulan, A. J.; Yang, Y.-S.; Zhou, J. Geometric and Electronic Structure/Function Correlations in Non-Heme Iron Enzymes. *Chem. Rev.* **2000**, *100* (1), 235-350.
(7) Bollinger Jr, J.; Chang, W.; Matthews, M.; Martinie, R.; Boal, A.; Krebs, C. 2-Oxoglutarate-dependent oxygenases. *RSC Metallobiology* **2015**.
(8) He, J.-B.; Wu, L.; Wei, W.; Meng, S.; Liu, Z.-T.; Wu, X.; Pan, H.-X.; Yang, S.; Liang, Y.; Zhou, J.; Tang, G.-L. Enzymatic catalysis favours eight-membered over five-membered ring closure in bicyclomycin biosynthesis. *Nat. Catal.* **2023**, *6* (7), 637-648.
(9) Agarwal, V.; Miles, Z. D.; Winter, J. M.; Eustáquio, A. S.; El Gamal, A. A.; Moore, B. S. Enzymatic halogenation and dehalogenation reactions: pervasive and mechanistically diverse. *Chem. Rev.* **2017**, *117* (8), 5619-5674.
(10) Latham, J.; Brandenburger, E.; Shepherd, S. A.; Menon, B. R.; Micklefield, J. Development of halogenase enzymes for use in synthesis. *Chem. Rev.* **2018**, *118* (1), 232-269.
(11) Vaillancourt, F. H.; Yin, J.; Walsh, C. T. SyrB2 in syringomycin E biosynthesis is a nonherne FeII α-ketoglutarate- and O2-dependent halogenase. *Proc. Natl. Acad. Sci. U.S.A.* **2005**, *102* (29), 10111-10116.
(12) Blasiak, L. C.; Vaillancourt, F. H.; Walsh, C. T.; Drennan, C. L. Crystal structure of the non-haem iron halogenase SyrB2 in syringomycin biosynthesis. *Nature* **2006**, *440* (7082), 368-371.
(13) Galonic, D. P.; Barr, E. W.; Walsh, C. T.; Bollinger, J. M.; Krebs, C. Two interconverting Fe(IV) intermediates in aliphatic chlorination by the halogenase CytC3. *Nat. Chem. Biol.* **2007**, *3* (2), 113-116.
(14) Riggs-Gelasco, P.; Galonic, D. P.; Barr, E. W.; Matthews, M. L.; Koch, G. M.; Yonce, J. R.; Bollinger, J. M.; Walsh, C. T.; Krebs, C. Characterization of an iron(IV) intermediate from the Fe(II)- and alpha-ketoglutarate-dependent halogenase CytC3. *J. Biol. Inorg. Chem.* **2007**, *12* (SUPPL 1), S88-S88.
(15) Hillwig, M. L.; Zhu, Q.; Ittiamornkul, K.; Liu, X. Discovery of a promiscuous non-heme iron halogenase in ambiguine alkaloid biogenesis: implication for an evolvable enzyme family for late-stage halogenation of aliphatic carbons in small molecules. *Angew. Chem. Int. Ed.* **2016**, *55* (19), 5780-5784.
(16) Mitchell, A. J.; Zhu, Q.; Maggiolo, A. O.; Ananth, N. R.; Hillwig, M. L.; Liu, X.; Boal, A. K. Structural basis for halogenation by iron-and 2-oxo-glutarate-dependent enzyme WelO5. *Nat. Chem. Biol.* **2016**, *12* (8), 636-640.
(17) Hillwig, M. L.; Liu, X. A new family of iron-dependent halogenases acts on freestanding substrates. *Nat. Chem. Biol.* **2014**, *10* (11), 921-923.
(18) Marchand, J. A.; Neugebauer, M. E.; Ing, M. C.; Lin, C. I.; Pelton, J. G.; Chang, M. C. Y. Discovery of a pathway for terminal-alkyne amino acid biosynthesis. *Nature* **2019**, *567* (7748), 420-424.
(19) Neugebauer, M. E.; Sumida, K. H.; Pelton, J. G.; McMurry, J. L.; Marchand, J. A.; Chang, M. C. Y. A family of radical halogenases for the engineering of amino-acid-based products. *Nat. Chem. Biol.* **2019**, *15* (10), 1009-1016.
(20) Jeffrey, W. S.; Monica, E. N.; Molly, J. M.; Debangsu, S.; Chi-Yun, L.; Bryce, J. K.; Amie, K. B.; Michelle, C. Y. C.; Alexey, S.; Carsten, K.; J. Martin Bollinger, Jr. Synergistic Binding of the Halide and Cationic Prime Substrate of the l-Lysine 4-Chlorinase, BesD, in Both Ferrous and Ferryl States. *bioRxiv* **2023**, 2023.2005.2002.539147.
(21) Zhao, C.; Yan, S.; Li, Q.; Zhu, H.; Zhong, Z.; Ye, Y.; Deng, Z.; Zhang, Y. An Fe(2+) - and alpha-Ketoglutarate-Dependent Halogenase Acts on Nucleotide Substrates. *Angew. Chem. Int. Ed.* **2020**, *59* (24), 9478-9484.
(22) Zhai, G.; Gong, R.; Lin, Y.; Zhang, M.; Li, J.; Deng, Z.; Sun, J.; Chen, W.; Zhang, Z. Structural Insight into the Catalytic Mechanism of Non-Heme Iron Halogenase AdaV in 2′-Chloropentostatin Biosynthesis. *ACS Catal.* **2022**, *12* (22), 13910-13920.
(23) Hausinger, R. P. Fe(II)/α-ketoglutarate-dependent hydroxylases and related enzymes. *Crit. Rev. Biochem. Mol. Biol.* **2004**, *39* (1), 21-68.
(24) Simmons, J. M.; Müller, T. A.; Hausinger, R. P. FeII/α-ketoglutarate hydroxylases involved in nucleobase, nucleoside, nucleotide, and chromatin metabolism. *Dalton. Trans.* **2008**, (38), 5132-5142.
(25) Mitchell, A. J.; Dunham, N. P.; Martinie, R. J.; Bergman, J. A.; Pollock, C. J.; Hu, K.; Allen, B. D.; Chang, W.-c.; Silakov, A.; Bollinger, J. M., Jr.; Krebs, C.; Boal, A. K. Visualizing the Reaction Cycle in an Iron(II)- and 2-(Oxo)-glutarate-Dependent Hydroxylase. *J. Am. Chem. Soc.* **2017**, *139* (39), 13830-13836.
(26) Price, J. C.; Barr, E. W.; Tirupati, B.; Bollinger, J. M.; Krebs, C. The First Direct Characterization of a High-Valent Iron Intermediate in the Reaction of an α-Ketoglutarate-Dependent Dioxygenase: A High-Spin Fe(IV) Complex in Taurine/α-Ketoglutarate Dioxygenase (TauD) from Escherichia coli. *Biochemistry* **2003**, *42* (24), 7497-7508.
(27) Riggs-Gelasco, P. J.; Price, J. C.; Guyer, R. B.; Brehm, J. H.; Barr, E. W.; Bollinger, J. M., Jr.; Krebs, C. EXAFS Spectroscopic Evidence for an Fe═O Unit in the Fe(IV) Intermediate Observed during Oxygen Activation by Taurine:α-Ketoglutarate Dioxygenase. *J. Am. Chem. Soc.* **2004**, *126* (26), 8108-8109.

(28) Hoffart, L. M.; Barr, E. W.; Guyer, R. B.; Bollinger, J. M.; Krebs, C. Direct spectroscopic detection of a C-H-cleaving high-spin Fe(IV) complex in a prolyl-4-hydroxylase. *Proc. Natl. Acad. Sci. U.S.A.* **2006**, *103* (40), 14738-14743.
(29) Krebs, C.; Galonic Fujimori, D.; Walsh, C. T.; Bollinger Jr, J. M. Non-heme Fe (IV)–oxo intermediates. *Acc. Chem. Res.* **2007**, *40* (7), 484-492.
(30) Hill, E. A.; Weitz, A. C.; Onderko, E.; Romero-Rivera, A.; Guo, Y.; Swart, M.; Bominaar, E. L.; Green, M. T.; Hendrich, M. P.; Lacy, D. C.; Borovik, A. S. Reactivity of an FeIV-Oxo Complex with Protons and Oxidants. *J. Am. Chem. Soc.* **2016**, *138* (40), 13143-13146.
(31) Srnec, M.; Iyer, S. R.; Dassama, L. M. K.; Park, K.; Wong, S. D.; Sutherlin, K. D.; Yoda, Y.; Kobayashi, Y.; Kurokuzu, M.; Saito, M.; Seto, M.; Krebs, C.; Bollinger, J. M., Jr.; Solomon, E. I. Nuclear Resonance Vibrational Spectroscopic Definition of the Facial Triad FeIV═O Intermediate in Taurine Dioxygenase: Evaluation of Structural Contributions to Hydrogen Atom Abstraction. *J. Am. Chem. Soc.* **2020**, *142* (44), 18886-18896.
(32) Matthews, M. L.; Krest, C. M.; Barr, E. W.; Vaillancourt, F. H.; Walsh, C. T.; Green, M. T.; Krebs, C.; Bollinger, J. M. Substrate-Triggered Formation and Remarkable Stability of the C–H Bond-Cleaving Chloroferryl Intermediate in the Aliphatic Halogenase, SyrB2. *Biochemistry* **2009**, *48* (20), 4331-4343.
(33) Martinie, R. J.; Livada, J.; Chang, W.-c.; Green, M. T.; Krebs, C.; Bollinger, J. M., Jr.; Silakov, A. Experimental Correlation of Substrate Position with Reaction Outcome in the Aliphatic Halogenase, SyrB2. *J. Am. Chem. Soc.* **2015**, *137* (21), 6912-6919.
(34) Pandian, S.; Vincent, M. A.; Hillier, I. H.; Burton, N. A. Why does the enzyme SyrB2 chlorinate, but does not hydroxylate, saturated hydrocarbons? A density functional theory (DFT) study. *Dalton. Trans.* **2009**, (31), 6201-6207.
(35) Kulik, H. J.; Blasiak, L. C.; Marzari, N.; Drennan, C. L. First-Principles Study of Non-heme Fe(II) Halogenase SyrB2 Reactivity. *J. Am. Chem. Soc.* **2009**, *131* (40), 14426-14433.
(36) Borowski, T.; Noack, H.; Radon, M.; Zych, K.; Siegbahn, P. E. M. Mechanism of Selective Halogenation by SyrB2: A Computational Study. *J. Am. Chem. Soc.* **2010**, *132* (37), 12887-12898.
(37) Huang, J.; Li, C.; Wang, B.; Sharon, D. A.; Wu, W.; Shaik, S. Selective Chlorination of Substrates by the Halogenase SyrB2 Is Controlled by the Protein According to a Combined Quantum Mechanics/Molecular Mechanics and Molecular Dynamics Study. *ACS Catal.* **2016**, *6* (4), 2694-2704.
(38) Wong, S. D.; Srnec, M.; Matthews, M. L.; Liu, L. V.; Kwak, Y.; Park, K.; Bell, C. B., 3rd; Alp, E. E.; Zhao, J.; Yoda, Y.; Kitao, S.; Seto, M.; Krebs, C.; Bollinger, J. M., Jr.; Solomon, E. I. Elucidation of the Fe(IV)=O intermediate in the catalytic cycle of the halogenase SyrB2. *Nature* **2013**, *499* (7458), 320-323.
(39) Srnec, M.; Wong, S. D.; Matthews, M. L.; Krebs, C.; Bollinger, J. M., Jr.; Solomon, E. I. Electronic Structure of the Ferryl Intermediate in the alpha-Ketoglutarate Dependent Non-Heme Iron Halogenase SyrB2: Contributions to H Atom Abstraction Reactivity. *J. Am. Chem. Soc.* **2016**, *138* (15), 5110-5122.
(40) Rugg, G.; Senn, H. M. Formation and structure of the ferryl [Fe O] intermediate in the non-haem iron halogenase SyrB2: classical and QM/MM modelling agree. *Phys. Chem. Chem. Phys.* **2017**, *19* (44), 30107-30119.
(41) Mehmood, R.; Qi, H. W.; Steeves, A. H.; Kulik, H. J. The Protein's Role in Substrate Positioning and Reactivity for Biosynthetic Enzyme Complexes: The Case of SyrB2/SyrB1. *ACS Catal.* **2019**, *9* (6), 4930-4943.
(42) Zhang, X.; Wang, Z.; Gao, J.; Liu, W. Chlorination versus hydroxylation selectivity mediated by the non-heme iron halogenase WelO5. *Phys. Chem. Chem. Phys.* **2020**, *22* (16), 8699-8712.
(43) Li, R. N.; Chen, S. L. Mechanism for the Halogenation and Azidation of Lysine Catalyzed by Non-heme Iron BesD Enzyme. *Chem. Asian. J.* **2022**, *17* (17).
(44) Mehmood, R.; Vennelakanti, V.; Kulik, H. J. Spectroscopically Guided Simulations Reveal Distinct Strategies for Positioning Substrates to Achieve Selectivity in Nonheme Fe(II)/α-Ketoglutarate-Dependent Halogenases. *ACS Catal.* **2021**, *11* (19), 12394-12408.
(45) Mitchell, A. J.; Dunham, N. P.; Bergman, J. A.; Wang, B.; Zhu, Q.; Chang, W. C.; Liu, X.; Boal, A. K. Structure-Guided Reprogramming of a Hydroxylase To Halogenate Its Small Molecule Substrate. *Biochemistry* **2017**, *56* (3), 441-444.
(46) Neugebauer, M. E.; Kissman, E. N.; Marchand, J. A.; Pelton, J. G.; Sambold, N. A.; Millar, D. C.; Chang, M. C. Y. Reaction pathway engineering converts a radical hydroxylase into a halogenase. *Nat. Chem. Biol.* **2022**, *18* (2), 171-179.
(47) Søndergaard, C. R.; Olsson, M. H. M.; Rostkowski, M.; Jensen, J. H. Improved Treatment of Ligands and Coupling Effects in Empirical Calculation and Rationalization of pKa Values. *J. Chem. Theory Comput.* **2011**, *7* (7), 2284-2295.
(48) Maier, J. A.; Martinez, C.; Kasavajhala, K.; Wickstrom, L.; Hauser, K. E.; Simmerling, C. ff14SB: Improving the Accuracy of Protein Side Chain and Backbone Parameters from ff99SB. *J. Chem. Theory Comput.* **2015**, *11* (8), 3696-3713.
(49) Li, P.; Merz, K. M., Jr. MCPB.py: A Python Based Metal Center Parameter Builder. *J. Chem. Inf. Model.* **2016**, *56* (4), 599-604.
(50) Li, P.; Merz, K. M., Jr. Metal Ion Modeling Using Classical Mechanics. *Chem. Rev.* **2017**, *117* (3), 1564-1686.
(51) Case, D. A.; Ben-Shalom, I. Y.; Brozell, S. R.; Cerutti, D. S.; Cheatham, T. E., III; Cruzeiro, V. W. D.; Darden, T. A.; Duke, R. E.; Ghoreishi, D.; Gilson, M. K.; Gohlke, H.; Goetz, A. W.; Greene, D.; Harris, R.; Homeyer, N.; Huang, Y.; Izadi, S.; Kovalenko, A.; Kurtzman, T.; Lee, T. S.; LeGrand, S.; Li, P.; Lin, C.; Liu, J.; Luchko, T.; Luo, R.; Mermelstein, D. J.; Merz, K. M.; Miao, Y.; Monard, G.; Nguyen, C.; Nguyen, H.; Omelyan, I.; Onufriev, A.; Pan, F.; Qi, R.; Roe, D. R.; Roitberg, A.; Sagui, C.; Schott-Verdugo, S.; Shen, J.; Simmerling, C. L.; Smith, J.; Salomon-Ferrer, R.; Swails, J.; Walker, R. C.; Wang, J.; Wei, H.; Wolf, R. M.; Wu, X.; Xiao, L.; York, D. M.; Kollman, P. A. AMBER,2018; University of California:San Francisco, 2018.
(52) Wang, J.; Wolf, R. M.; Caldwell, J. W.; Kollman, P. A.; Case, D. A. Development and testing of a general amber force field. *J. Comput. Chem.* **2004**, *25* (9), 1157-1174.
(53) Bayly, C. I.; Cieplak, P.; Cornell, W.; Kollman, P. A. A well-behaved electrostatic potential based method using charge restraints for deriving atomic charges: the RESP model. *J. Phy. Chem.* **1993**, *97* (40), 10269-10280.
(54) Metz, S.; Kästner, J.; Sokol, A.; Keal, T.; Sherwood, P. Wiley Interdiscip. *Wiley Interdiscip. Rev. Comput. Mol. Sci.* **2014**, *4* (2), 101-110.
(55) Lu, Y.; Sen, K.; Yong, C.; Gunn, D. S. D.; Purton, J. A.; Guan, J.; Desmoutier, A.; Abdul Nasir, J.; Zhang, X.; Zhu, L.; Hou, Q.; Jackson-Masters, J.; Watts, S.; Hanson, R.; Thomas, H. N.; Jayawardena, O.; Logsdail, A. J.; Woodley, S. M.; Senn, H. M.; Sherwood, P.; Catlow, C. R. A.; Sokol, A. A.; Keal, T. W. Multiscale QM/MM modelling of catalytic systems with ChemShell. *Phys. Chem. Chem. Phys.* **2023**, *25* (33), 21816-21835.
(56) Ahlrichs, R.; Bär, M.; Häser, M.; Horn, H.; Kölmel, C. Electronic structure calculations on workstation computers: The program system turbomole. *Chem. Phys. Lett.* **1989**, *162* (3), 165-169.
(57) Smith, W.; Forester, T. DL_POLY_2. 0: A general-purpose parallel molecular dynamics simulation package. *J. Mol. Graph.* **1996**, *14* (3), 136-141.
(58) Bakowies, D.; Thiel, W. Hybrid models for combined quantum mechanical and molecular mechanical approaches. *J. Phy. Chem.* **1996**, *100* (25), 10580-10594.
(59) Lee, C.; Yang, W.; Parr, R. G. Development of the Colle-Salvetti correlation-energy formula into a functional of the electron density. *Phys. Rev. B* **1988**, *37* (2), 785.
(60) Becke, A. D. Density-functional thermochemistry. II. The effect of the Perdew–Wang generalized-gradient correlation correction. *J. Chem. Phys.* **1992**, *97* (12), 9173-9177.
(61) Becke, A. D. Density-functional thermochemistry. III. The role of exact exchange. *J. Chem. Phys.* **1993**, *98* (7), 5648-5652.
(62) Fang, D.; Cisneros, G. A. Alternative Pathway for the Reaction Catalyzed by DNA Dealkylase AlkB from Ab Initio QM/MM Calculations. *J. Chem. Theory Comput.* **2014**, *10* (11), 5136-5148.

(63) Ghafoor, S.; Mansha, A.; de Visser, S. P. Selective Hydrogen Atom Abstraction from Dihydroflavonol by a Nonheme Iron Center Is the Key Step in the Enzymatic Flavonol Synthesis and Avoids Byproducts. *J. Am. Chem. Soc.* **2019**, *141* (51), 20278-20292.
(64) Xue, J.; Lu, J.; Lai, W. Mechanistic insights into a non-heme 2-oxoglutarate-dependent ethylene-forming enzyme: selectivity of ethylene-formation versusl-Arg hydroxylation. *Phys. Chem. Chem. Phys.* **2019**, *21* (19), 9957-9968, 10.1039/C9CP00794F.
(65) Waheed, S. O.; Ramanan, R.; Chaturvedi, S. S.; Lehnert, N.; Schofield, C. J.; Christov, C. Z.; Karabencheva-Christova, T. G. Role of Structural Dynamics in Selectivity and Mechanism of Non-heme Fe(II) and 2-Oxoglutarate-Dependent Oxygenases Involved in DNA Repair. *ACS Cent. Sci.* **2020**, *6* (5), 795-814.
(66) Chaturvedi, S. S.; Ramanan, R.; Hu, J.; Hausinger, R. P.; Christov, C. Z. Atomic and Electronic Structure Determinants Distinguish between Ethylene Formation and l-Arginine Hydroxylation Reaction Mechanisms in the Ethylene-Forming Enzyme. *ACS Catal.* **2021**, *11* (3), 1578-1592.
(67) Wojdyla, Z.; Borowski, T. Properties of the Reactants and Their Interactions within and with the Enzyme Binding Cavity Determine Reaction Selectivities. The Case of Fe(II)/2-Oxoglutarate Dependent Enzymes. *Chem. Eur. J.* **2022**, *28* (18), e202104106.
(68) Wu, L.; Wang, Z.; Cen, Y.; Wang, B.; Zhou, J. Structural Insight into the Catalytic Mechanism of the Endoperoxide Synthase FtmOx1. *Angew. Chem. Int. Ed.* **2022**, *61* (12), e202112063.
(69) Ali, H. S.; Warwicker, J.; de Visser, S. P. How Does the Nonheme Iron Enzyme NapI React through l-Arginine Desaturation Rather Than Hydroxylation? A Quantum Mechanics/Molecular Mechanics Study. *ACS Catal.* **2023**, *13* (16), 10705-10721.
(70) Cao, Y.; Valdez-Moreira, J. A.; Hay, S.; Smith, J. M.; de Visser, S. P. Reactivity Differences of Trigonal Pyramidal Nonheme Iron(IV)-Oxo and Iron(III)-Oxo Complexes: Experiment and Theory. *Chem. Eur. J.* **2023**, *29* (42), e202300271.
(71) Joy, J.; Ess, D. H. Direct Dynamics Trajectories Demonstrate Dynamic Matching and Nonstatistical Radical Pair Intermediates during Fe-Oxo-Mediated C–H Functionalization Reactions. *J. Am. Chem. Soc.* **2023**, *145* (13), 7628-7637.
(72) Li, A.; Wang, Q.; Song, X.; Zhang, X.; Huang, J.-W.; Chen, C.-C.; Guo, R.-T.; Wang, B.; Reetz, M. T. Engineering of a P450-based Kemp eliminase with a new mechanism. *Chinese J. Catal.* **2023**, *47*, 191-199.
(73) Paris, J. C.; Hu, S.; Wen, A.; Weitz, A. C.; Cheng, R.; Gee, L. B.; Tang, Y.; Kim, H.; Vegas, A.; Chang, W.-c.; Elliott, S. J.; Liu, P.; Guo, Y. An S=1 Iron(IV) Intermediate Revealed in a Non-Heme Iron Enzyme-Catalyzed Oxidative C–S Bond Formation. *Angew. Chem. Int. Ed.* **2023**, *62* (43), e202309362.
(74) Rifayee, S. B. J. S.; Chaturvedi, S. S.; Warner, C.; Wildey, J.; White, W.; Thompson, M.; Schofield, C. J.; Christov, C. Z. Catalysis by KDM6 Histone Demethylases – A Synergy between the Non-Heme Iron(II) Center, Second Coordination Sphere, and Long-Range Interactions. *Chem. Eur. J.* **2023**, *29* (51), e202301305.
(75) Weigend, F.; Ahlrichs, R. Balanced basis sets of split valence, triple zeta valence and quadruple zeta valence quality for H to Rn: Design and assessment of accuracy. *Phys. Chem. Chem. Phys.* **2005**, *7* (18), 3297-3305.
(76) Grimme, S. Semiempirical GGA-type density functional constructed with a long-range dispersion correction. *J. Comput. Chem.* **2006**, *27* (15), 1787-1799.
(77) Grimme, S.; Antony, J.; Ehrlich, S.; Krieg, H. A consistent and accurate ab initio parametrization of density functional dispersion correction (DFT-D) for the 94 elements H-Pu. *J. Chem. Phys.* **2010**, *132* (15), 154104.
(78) Grimme, S.; Ehrlich, S.; Goerigk, L. Effect of the damping function in dispersion corrected density functional theory. *J. Comput. Chem.* **2011**, *32* (7), 1456-1465.
(79) Diebold, A. R.; Brown-Marshall, C. D.; Neidig, M. L.; Brownlee, J. M.; Moran, G. R.; Solomon, E. I. Activation of α-Keto Acid-Dependent Dioxygenases: Application of an {FeNO}7/{FeO2}8 Methodology for Characterizing the Initial Steps of O2 Activation. *J. Am. Chem. Soc.* **2011**, *133* (45), 18148-18160.
(80) Shaik, S.; Chen, H.; Janardanan, D. Exchange-enhanced reactivity in bond activation by metal–oxo enzymes and synthetic reagents. *Nat. Chem.* **2011**, *3* (1), 19-27.
(81) Ye, S.; Riplinger, C.; Hansen, A.; Krebs, C.; Bollinger Jr, J. M.; Neese, F. Electronic Structure Analysis of the Oxygen-Activation Mechanism by FeII- and α-Ketoglutarate (αKG)-Dependent Dioxygenases. *Chem. Eur. J.* **2012**, *18* (21), 6555-6567.
(82) Fang, D.; Lord, R. L.; Cisneros, G. A. Ab Initio QM/MM Calculations Show an Intersystem Crossing in the Hydrogen Abstraction Step in Dealkylation Catalyzed by AlkB. *J. Phys. Chem. B.* **2013**, *117* (21), 6410-6420.
(83) Quesne, M. G.; Latifi, R.; Gonzalez-Ovalle, L. E.; Kumar, D.; de Visser, S. P. Quantum Mechanics/Molecular Mechanics Study on the Oxygen Binding and Substrate Hydroxylation Step in AlkB Repair Enzymes. *Chem. Eur. J.* **2014**, *20* (2), 435-446.
(84) Cortopassi, W. A.; Simion, R.; Honsby, C. E.; Franca, T. C.; Paton, R. S. Dioxygen Binding in the Active Site of Histone Demethylase JMJD2A and the Role of the Protein Environment. *Chemistry* **2015**, *21* (52), 18983-18992.
(85) Quesne, M. G.; Borowski, T.; de Visser, S. P. Quantum Mechanics/Molecular Mechanics Modeling of Enzymatic Processes: Caveats and Breakthroughs. *Chem. Eur. J.* **2016**, *22* (8), 2562-2581.
(86) Bai, J.; Yan, L.; Liu, Y. Catalytic mechanism of the PrhA (V150L/A232S) double mutant involved in the fungal meroterpenoid biosynthetic pathway: a QM/MM study. *Phys. Chem. Chem. Phys.* **2019**, *21* (46), 25658-25668, 10.1039/C9CP03565F.
(87) Liu, H.; Llano, J.; Gauld, J. W. A DFT Study of Nucleobase Dealkylation by the DNA Repair Enzyme AlkB. *J. Phys. Chem. B.* **2009**, *113* (14), 4887-4898.
(88) Song, X.; Lu, J.; Lai, W. Mechanistic insights into dioxygen activation, oxygen atom exchange and substrate epoxidation by AsqJ dioxygenase from quantum mechanical/molecular mechanical calculations. *Phys. Chem. Chem. Phys.* **2017**, *19* (30), 20188-20197.
(89) Zhang, J.; Wu, P.; Zhang, X.; Wang, B. Coordination Dynamics of Iron is a Key Player in the Catalysis of Non-heme Enzymes. *ChemBioChem* **2023**, *24* (14), e202300119.
(90) Ye, S.; Neese, F. Quantum chemical studies of C–H activation reactions by high-valent nonheme iron centers. *Curr. Opin. Chem. Biol.* **2009**, *13* (1), 89-98.
(91) Janardanan, D.; Wang, Y.; Schyman, P.; Que Jr, L.; Shaik, S. The Fundamental Role of Exchange-Enhanced Reactivity in C H Activation by S=2 Oxo Iron(IV) Complexes. *Angew. Chem. Int. Ed.* **2010**, *49* (19), 3342-3345.
(92) Usharani, D.; Janardanan, D.; Li, C.; Shaik, S. A Theory for Bioinorganic Chemical Reactivity of Oxometal Complexes and Analogous Oxidants: The Exchange and Orbital-Selection Rules. *Acc. Chem. Res.* **2013**, *46* (2), 471-482.
(93) Wang, B.; Wu, P.; Shaik, S. Critical Roles of Exchange and Superexchange Interactions in Dictating Electron Transfer and Reactivity in Metalloenzymes. *J. Phys. Chem. Lett.* **2022**, *13* (13), 2871-2877.
(94) Perdew, J. P.; Kurth, S.; Zupan, A.; Blaha, P. Accurate Density Functional with Correct Formal Properties: A Step Beyond the Generalized Gradient Approximation. *Phys. Rev. Lett.* **1999**, *82* (12), 2544-2547.
(95) Perdew, J. P.; Tao, J.; Staroverov, V. N.; Scuseria, G. E. Meta-generalized gradient approximation: Explanation of a realistic nonempirical density functional. *J. Chem. Phys.* **2004**, *120* (15), 6898-6911.
(96) Zhao, Y.; Truhlar, D. G. The M06 suite of density functionals for main group thermochemistry, thermochemical kinetics, noncovalent interactions, excited states, and transition elements: two new functionals and systematic testing of four M06-class functionals and 12 other functionals. *Theor. Chem. Acc.* **2007**, *120* (1-3), 215-241.
(97) Perdew, J. P.; Ernzerhof, M.; Burke, K. Rationale for mixing exact exchange with density functional approximations. *J. Chem. Phys.* **1996**, *105* (22), 9982-9985.

(98) Perdew, J. P. Density-functional approximation for the correlation energy of the inhomogeneous electron gas. *Phys. Rev. B* **1986**, *33* (12), 8822-8824.
(99) Becke, A. D. Density-functional exchange-energy approximation with correct asymptotic behavior. *Phys. Rev. A* **1988**, *38* (6), 3098-3100.
(100) Khare, D.; Wang, B.; Gu, L.; Razelun, J.; Sherman, D. H.; Gerwick, W. H.; Håkansson, K.; Smith, J. L. Conformational switch triggered by α-ketoglutarate in a halogenase of curacin A biosynthesis. *Proc. Natl. Acad. Sci. U.S.A.* **2010**, *107* (32), 14099-14104.
(101) Krebs, C.; Price, J. C.; Baldwin, J.; Saleh, L.; Green, M. T.; Bollinger, J. M. Rapid Freeze-Quench 57Fe Mössbauer Spectroscopy: Monitoring Changes of an Iron-Containing Active Site during a Biochemical Reaction. *Inorg. Chem.* **2005**, *44* (4), 742-757.
(102) Sinnecker, S.; Svensen, N.; Barr, E. W.; Ye, S.; Bollinger, J. M., Jr.; Neese, F.; Krebs, C. Spectroscopic and Computational Evaluation of the Structure of the High-Spin Fe(IV)-Oxo Intermediates in Taurine: α-Ketoglutarate Dioxygenase from Escherichia coli and Its His99Ala Ligand Variant. *J. Am. Chem. Soc.* **2007**, *129* (19), 6168-6179.
(103) Bunno, R.; Awakawa, T.; Mori, T.; Abe, I. Aziridine Formation by a Fe(II) /alpha-Ketoglutarate Dependent Oxygenase and 2-Aminoisobutyrate Biosynthesis in Fungi. *Angew. Chem. Int. Ed.* **2021**, *60* (29), 15827-15831.
(104) Tao, H.; Ushimaru, R.; Awakawa, T.; Mori, T.; Uchiyama, M.; Abe, I. Stereoselectivity and Substrate Specificity of the Fe(II)/alpha-Ketoglutarate-Dependent Oxygenase TqaL. *J. Am. Chem. Soc.* **2022**, *144* (47), 21512-21520.
(105) Cha, L.; Paris, J. C.; Zanella, B.; Spletzer, M.; Yao, A.; Guo, Y.; Chang, W.-c. Mechanistic Studies of Aziridine Formation Catalyzed by Mononuclear Non-Heme Iron Enzymes. *J. Am. Chem. Soc.* **2023**, *145* (11), 6240-6246.
(106) Wu, P.; Gu, Y.; Liao, L.; Wu, Y.; Jin, J.; Wang, Z.; Zhou, J.; Shaik, S.; Wang, B. Coordination Switch Drives Selective C−S Bond Formation by the Non-Heme Sulfoxide Synthases**. *Angew. Chem. Int. Ed.* **2022**, *61* (50), e202214235.
(107) Paris, J. C.; Hu, S.; Wen, A.; Weitz, A. C.; Cheng, R.; Gee, L. B.; Tang, Y.; Kim, H.; Vegas, A.; Chang, W.-c.; Elliott, S. J.; Liu, P.; Guo, Y. An S=1 Iron(IV) Intermediate Revealed in a Non-Heme Iron Enzyme-Catalyzed Oxidative C−S Bond Formation. *Angew. Chem. Int. Ed.* **2023**, *135* (43), e202309362.
(108) Brunson, J. K.; McKinnie, S. M. K.; Chekan, J. R.; McCrow, J. P.; Miles, Z. D.; Bertrand, E. M.; Bielinski, V. A.; Luhavaya, H.; Oborník, M.; Smith, G. J.; Hutchins, D. A.; Allen, A. E.; Moore, B. S. Biosynthesis of the neurotoxin domoic acid in a bloom-forming diatom. *Science* **2018**, *361* (6409), 1356-1358.
(109) Chen, T.-Y.; Xue, S.; Tsai, W.-C.; Chien, T.-C.; Guo, Y.; Chang, W.-c. Deciphering Pyrrolidine and Olefin Formation Mechanism in Kainic Acid Biosynthesis. *ACS Catal.* **2021**, *11* (1), 278-282.
(110) Li, X.; Xue, S.; Guo, Y.; Chang, W.-c. Mechanism of Methyldehydrofosmidomycin Maturation: Use Olefination to Enable Chain Elongation. *J. Am. Chem. Soc.* **2022**, *144* (18), 8257-8266.
(111) Tang, H.; Wu, M.-H.; Lin, H.-Y.; Han, M.-R.; Tu, Y.-H.; Yang, Z.-J.; Chien, T.-C.; Chan, N.-L.; Chang, W.-c. Mechanistic analysis of carbon–carbon bond formation by deoxypodophyllotoxin synthase. *Proc. Natl. Acad. Sci. U.S.A.* **2022**, *119* (1), e2113770119.
(112) Ushimaru, R.; Cha, L.; Shimo, S.; Li, X.; Paris, J. C.; Mori, T.; Miyamoto, K.; Coffer, L.; Uchiyama, M.; Guo, Y.; Chang, W.-c.; Abe, I. Mechanistic Analysis of Stereodivergent Nitroalkane Cyclopropanation Catalyzed by Nonheme Iron Enzymes. *J. Am. Chem. Soc.* **2023**.
(113) McCulloch, K. M.; McCranie, E. K.; Smith, J. A.; Sarwar, M.; Mathieu, J. L.; Gitschlag, B. L.; Du, Y.; Bachmann, B. O.; Iverson, T. M. Oxidative cyclizations in orthosomycin biosynthesis expand the known chemistry of an oxygenase superfamily. *Proc. Natl. Acad. Sci. U.S.A.* **2015**, *112* (37), 11547-11552.
(114) Meng, S.; Tang, G. L.; Pan, H. X. Enzymatic Formation of Oxygen-Containing Heterocycles in Natural Product Biosynthesis. *Chembiochem* **2018**, *19* (19), 2002-2022.
(115) Pan, J.; Bhardwaj, M.; Zhang, B.; Chang, W. C.; Schardl, C. L.; Krebs, C.; Grossman, R. B.; Bollinger, J. M., Jr. Installation of the Ether Bridge of Lolines by the Iron- and 2-Oxoglutarate-Dependent Oxygenase, LolO: Regio- and Stereochemistry of Sequential Hydroxylation and Oxacyclization Reactions. *Biochemistry* **2018**, *57* (14), 2074-2083.
(116) Pan, J.; Wenger, E. S.; Matthews, M. L.; Pollock, C. J.; Bhardwaj, M.; Kim, A. J.; Allen, B. D.; Grossman, R. B.; Krebs, C.; Bollinger, J. M., Jr. Evidence for Modulation of Oxygen Rebound Rate in Control of Outcome by Iron(II)- and 2-Oxoglutarate-Dependent Oxygenases. *J. Am. Chem. Soc.* **2019**, *141* (38), 15153-15165.
(117) Ali, H. S.; Henchman, R. H.; Visser, S. P. Mechanism of Oxidative Ring-Closure as Part of the Hygromycin Biosynthesis Step by a Nonheme Iron Dioxygenase. *ChemCatChem* **2021**, *13* (13), 3054-3066.
(118) Wojdyla, Z.; Borowski, T. Enzyme Multifunctionality by Control of Substrate Positioning Within the Catalytic Cycle-A QM/MM Study of Clavaminic Acid Synthase. *Chemistry* **2021**, *27* (6), 2196-2211.
(119) Gama, S. R.; Stankovic, T.; Hupp, K.; Al Hejami, A.; McClean, M.; Evans, A.; Beauchemin, D.; Hammerschmidt, F.; Pallitsch, K.; Zechel, D. L. Biosynthesis of the Fungal Organophosphonate Fosfonochlorin Involves an Iron(II) and 2-(Oxo)glutarate Dependent Oxacyclase. *Chembiochem* **2022**, *23* (2), e202100352.
(120) Liu, X.; Yuan, Z.; Su, H.; Hou, X.; Deng, Z.; Xu, H.; Guo, B.; Yin, D.; Sheng, X.; Rao, Y. Molecular Basis of the Unusual Seven-Membered Methylenedioxy Bridge Formation Catalyzed by Fe(II)/α-KG-Dependent Oxygenase CTB9. *ACS Catal.* **2022**, *12* (6), 3689-3699.
(121) Panth, N.; Wenger, E. S.; Krebs, C.; Bollinger, J. M., Jr.; Grossman, R. B. Synthesis of 6,6- and 7,7-Difluoro-1-acetamidopyrrolizidines and Their Oxidation Catalyzed by the Nonheme Fe Oxygenase LolO. *Chembiochem* **2022**, *23* (13), e202200081.

Insert Table of Contents artwork here